,
Prepared for submission to JCAP

The Physics Reach of the PTOLEMY Project

E. Baracchini,[c] **M.G. Betti,**[k] **M. Biasotti,**[e] **F. Calle,**[p] **J. Carabe-Lopez,**[n] **G. Cavoto,**[j,k] **C. Chang,**[v,w] **A.G. Cocco,**[g] **A.P. Colijn,**[m] **J. Conrad,**[r] **N. D'Ambrosio,**[b] **P.F. de Salas,**[q] **M. Faverzani**[f] **A. Ferella,**[r] **E. Ferri,**[f] **P. Garcia-Abia,**[n] **G. Garcia Gomez-Tejedor,**[o] **S. Gariazzo,**[q] **F. Gatti,**[e] **C. Gentile,**[y] **A. Giachero,**[f] **J. Godmundsson,**[r] **Y. Hochberg,**[a] **Y. Kahn,**[z] **M. Lisanti,**[z] **C. Mancini-Terracciano,**[j] **G. Mangano,**[g] **L.E. Marcucci,**[i] **C. Mariani,**[k] **G. Mazzitelli,**[d] **M. Messina,**[c,t] **A. Molinero-Vela,**[n] **E. Monticone,**[l] **A. Nucciotti,**[f] **F. Pandolfi,**[j] **S. Pastor,**[q] **C. Pérez de los Heros,**[s] **O. Pisanti,**[g,h] **A. Polosa,**[j,k] **A. Puiu,**[f] **M. Rajteri,**[l] **R. Santorelli,**[n] **K. Schaeffner,**[c] **C.G. Tully,**[z] **Y. Raitses,**[y] **N. Rossi,**[j] **F. Zhao,**[z] **K.M. Zurek**[u,v]

[a]Racah Institute of Physics, Hebrew University of Jerusalem, Jerusalem, Israel
[b]INFN Laboratori Nazionali del Gran Sasso, L'Aquila, Italy
[c]Gran Sasso Science Institute (GSSI), L'Aquila, Italy
[d]INFN Laboratori Nazionali di Frascati, Frascati, Italy
[e]Università degli Studi di Genova e INFN Sezione di Genova, Genova, Italy
[f]Università degli Studi di Milano-Bicocca e INFN Sezione di Milano-Bicocca, Milano, Italy
[g]INFN Sezione di Napoli, Napoli, Italy
[h]Università degli Studi di Napoli Federico II, Napoli, Italy
[i]Università degli Studi di Pisa e INFN Sezione di Pisa, Pisa, Italy
[j]INFN Sezione di Roma, Roma, Italy
[k]Università degli Studi di Roma La Sapienza, Roma, Italy
[l]Istituto Nazionale di Ricerca Metrologica (INRiM), Torino, Italy
[m]Nationaal instituut voor subatomaire fysica (NIKHEF), Amsterdam, Netherlands
[n]Centro de Investigaciones Energéticas, Medioambientales y Tecnológicas (CIEMAT), Madrid, Spain
[o]Consejo Superior de Investigaciones Cientificas (CSIC), Madrid, Spain
[p]Universidad Politécnica de Madrid, Madrid, Spain
[q]Instituto de Física Corpuscular (CSIC-Univ. de València), Valencia, Spain
[r]Stockholm University, Stockholm, Sweden
[s]Uppsala University, Uppsala, Sweden

[t]New York University Abu Dhabi, Abu Dhabi, UAE
[u]Lawrence Berkeley National Laboratory, University of California, Berkeley, CA, USA
[v]Department of Physics, University of California, Berkeley, CA, USA
[w]Argonne National Laboratory, Chicago, IL, USA
[x]Kavli Institute for Cosmological Physics, University of Chicago, Chicago, IL, USA
[y]Princeton Plasma Physics Laboratory, Princeton, NJ, USA
[z]Department of Physics, Princeton University, Princeton, NJ, USA

Abstract. In this paper the physics reaches of the PTOLEMY project are presented. While the prime topic of the paper is about the detection of the Cosmological Relic Neutrinos, and all possible neutral particles coupled to the ν_e quantum state, a relevant attention is put also on some aspect of the technology, of the PTOLEMY project, which might be used for direct Dark Matter search in the region of low masse particles constituting the Dark Matter.

Contents

1 Physics cases

The PTOLEMY project aims to develop a scalable design for a CNB telescope, the first of its kind and the only one conceived that can look directly at the image encoded in neutrino background produced in the first second after the Big Bang. The scope of work for the next three years is to complete the design of the Cosmic Neutrino Telescope and to validate with direct measurement that the non-neutrino backgrounds are below the expected signal from the Big Bang. An array of telescopes of this design will reach discovery sensitivity for the Cosmic Neutrino Background. The number and deployment of these telescopes around the world will depend on the next phase of PTOLEMY developments described in this proposal. Yet, the physics case of the experiment is quite wide, including as another major goal, the measurement of the standard neutrino absolute mass scale, which is also the aim of the KATRIN experiment [**?**].

Moreover, some non standard scenarios could be tested. For example, it has been suggested that targets of graphene layers or nanotubes could be used for directional detection of DM candidates with mass in the MeV range [**?** **?**]. Another interesting issue concerns the physics of sterile neutrino states with masses both in the eV and keV mass ranges. Sterile eV neutrinos which mix with active states have been suggested since the LSND results to solve some anomalies in neutrino oscillation experiments (short baseline data, reactor anomaly and gallium anomaly) [**?**] and their existence would lead to cosmological implications, see e.g. [**?**], On the other hand neutrino states with a mass in the keV range are excellent warm DM candidates [**?** **?**]. Of course, one of the key ingredients for reliable predictions for the expected signals is a precise determination of polarized and unpolarized tritium weak processes.

2 "Ab initio" calculation of ^{3}H decay and ν capture

The three-nucleon systems have been the object of intense theoretical studies since many years. They represent an ideal "laboratory" to test our understanding of how nucleons interact among themselves, as well as with external electroweak probes. In order to do so, the three-body Schrödinger equation has to be solved exactly. Nowadays, a variety of methods exists to this aim. Among these, we plan to use one of the most accurate ones, the so-called Hyperspherical Harmonics (HH) method (see Ref. [**?**] and references therein).

Once the $A = 3$ quantum mechanical problem is solved, the only inputs of the calculation are the models for the nuclear interaction and nuclear electroweak currents, which are put under test. We here focus on weak processes, which require the construction of a realistic model for the nuclear axial current operator. Historically, the models for the nuclear interaction and currents have been derived within two different frameworks: a purely phenomenological one, and, more recently, the so-called chiral effective field theory approach (χEFT) (see Ref. [**?**] and references therein). The advantages of the latter are essentially two: (i) it allows to connect (low-energy) nuclear physics with the (high-energy) underlying theory of Quantum Chromodynamics; (ii) being essentially a perturbative expansion truncated at a given order, it is possible to estimate the theoretical uncertainty. Any realistic model for the nuclear axial current, phenomenological or χEFT, consists of one- and two-body contributions, the latter having its strength fitted to the (unpolarized) ^{3}H β-decay half-life. At this point, (unpolarized) ^{3}H β-decay is reproduced by a fit, but for any other weak process the theoretical study is pure prediction. The outlined approach is usually called "ab-initio" approach. We plan to use this ab-initio approach in order to study the following processes, and to verify whether they can be sensitive, and if so to which extent, to neutrino masses.

2.1 Polarized ^{3}H β-decay

In this case, the decay rate can be written as [**?**]

$$\frac{d\Gamma_\beta}{dE_e d\Omega_e d\Omega_\nu} = \frac{G_F^2}{(2\pi)^5} p_e E_e (\Delta m - E_e)^2 \xi [1 + a\boldsymbol{\beta}\cdot\hat{\boldsymbol{\nu}} + \hat{\mathbf{P}}\cdot(A\boldsymbol{\beta} + B\hat{\boldsymbol{\nu}})] \,, \tag{2.1}$$

where G_F is the Fermi constant, Δm is the difference between the ^{3}H and ^{3}He mass, p_e (E_e) is the electron momentum (energy), $\boldsymbol{\beta}$ ($\boldsymbol{\nu}$) is the electron (neutrino) three-velocity, and $\hat{\mathbf{P}}$ is the ^{3}H polarization versor. The quantities ξ, a, A and B contain the nuclear matrix elements, and can be written in terms of the "standard" Fermi (F) and Gamow-Teller (GT) matrix elements as

$$\xi = |F|^2 + g_A^2 |GT|^2 \,, \tag{2.2}$$

$$a\,\xi = |F|^2 - \frac{g_A^2}{3}|GT|^2 \,, \tag{2.3}$$

$$A\,\xi = -\frac{2}{3} g_A^2 |GT|^2 + \frac{2}{\sqrt{3}}|GT||F| \,, \tag{2.4}$$

$$B\,\xi = +\frac{2}{3} g_A^2 |GT|^2 + \frac{2}{\sqrt{3}}|GT||F| \,. \tag{2.5}$$

Note that by measuring the unpolarized ^{3}H β-decay rate, we have access only to ξ, while exploiting the polarized process, all other quantities become available and theory can be put under a stringent test. Furthermore, we plan to investigate to which extent the various quantities defined in Eqs. (2.2)–(2.5), which are obtained neglecting the neutrino mass, could be sensitive to it.

2.2 Neutrino capture on ^{3}H

The unpolarized rate can also be studied within an ab-initio approach. However, as already shown in [**?**], the cross section is basically related to the ^{3}H β-decay rate. We have in fact confirmed this by direct calculation, using the F and GT matrix elements predicted by theory.

As for the polarized process, we plan to compute the capture cross section following the steps used to obtain Eq. (2.1). The theoretical results for the cross section obtained within the ab-initio approach will represent predictions with which the PTOLEMY experiment can confront in order to check whether it can be measured or not. This is essentially a feasibility study.

3 Neutrino Physics

3.1 Cosmological neutrinos

The Universe has expanded by a factor of over one billion between the present-day and the early thermal epoch known as the neutrino decoupling. We observe this dynamics in many forms: the recession of galaxies (Hubble Expansion), the dim afterglow of the hot plasma epoch, the Cosmic Microwave Background (CMB), and the abundances of light elements during Big Bang Nucleosynthesis (BBN). The epoch of neutrino decoupling produced a fourth pillar of confirmation, the Cosmic Neutrino Background (CNB), perhaps one of the most important not-yet-probed predictions of the standard cosmological model. These early universe relics have cooled under the expansion of the Universe and are sensed indirectly through the action of their diminishing thermal velocities on large-scale structure formation. Experimental advances both in the understanding of massive neutrino physics and in techniques of high sensitivity instrumentation have opened up new opportunities to directly detect the CNB, an achievement which would profoundly confront and extend the sensitivity of precision cosmology data.

Because of the similarities shared with the CMB, its properties are theoretically expected to be very close to those of the photon background, but not entirely equal. Apart from the obvious difference coming from statistics, it is well known (again only theoretically) that the CNB spectrum deviates from that obtained from a fluid following a perfect Fermi-Dirac distribution at the percent level [**?** **?**]. The reason is the partial coincidence of the last moments of neutrino decoupling and the first instants of $e^{\pm}$ annihilations in the primeval plasma. In addition, massive neutrinos became non-relativistic at a certain time, depending on their absolute masses, and that allowed the possibility of being gravitationally trapped under the effect of large enough gravitational potentials [**?** **?**].

PTOLEMY is based on the detection of the CNB by the process of neutrino capture on β-unstable nuclei [**?** **?**]. In case of tritium

$$\nu_e + {}^3\mathrm{H} \rightarrow {}^3\mathrm{He} + e^-. \tag{3.1}$$

In fact, tritium has been chosen among other target candidates because of its availability, lifetime, high neutrino capture cross section and low Q-value [**?**]. The smoking gun signature of a relic neutrino capture is a peak in the electron spectrum above the β decay endpoint.

Because flavour neutrino eigenstates are a composition of mass eigenstates with different masses, relic neutrinos quickly decohere into those, in a time scale less than one Hubble time

[?]. Therefore, the capture rate of relic neutrinos by their absorption in tritium

$$\Gamma_{\rm CNB} = \sum_{i=1}^{N_\nu} \Gamma_i \,, \tag{3.2}$$

must be computed from the capture rates of the neutrino mass eigenstates Γ_i. Following Ref. [?] it can be obtained

$$\Gamma_i = \bar{\sigma}\, N_T\, |U_{ei}|^2\, f_{c,i}\, n_0. \tag{3.3}$$

The different variables appearing in this expression are going to be explained next.

The factor $\bar{\sigma}$ represents the cross section for the decay and the neutrino capture,

$$\bar{\sigma} = \frac{G_F^2}{2\pi} F(Z, E_e) \frac{m_{^3\rm He}}{m_{^3\rm H}} E_e p_e \left(|F|^2 + g_A^2 |GT|^2\right). \tag{3.4}$$

The terms $m_{^3\rm He} \approx 2808.391\,\text{MeV}$ and $m_{^3\rm H} \approx 2808.921\,\text{MeV}$ are the *nuclear* [1] masses of ^{3}He and ^{3}H nuclei, respectively. The Fermi function $F(Z, E_e)$ describes the effect of the Coulomb attraction between a proton and the outgoing electron, which enhances the cross section. In order to account for this effect we use the approximation due to Primakoff and Rosen [?],

$$F(Z, E_e) = \frac{2\pi\eta}{1 - \exp(-2\pi\eta)}, \tag{3.5}$$

where $\eta = Z\alpha E_e/p_e$, $Z = 2$ is the atomic number of ^{3}He and $\alpha = 1/137.036$ [?] is the fine structure constant. The factor $N_T = M_T/m_{^3\rm H}$ in expression (3.3) is approximately the number of tritium nuclei in a sample of M_T mass of this element. Notice the presence of the mixing matrix element U_{ei} in the partial rate Γ_i. This is due to the fact that only electron neutrinos intervene in the process (3.1), while relic neutrinos are found in their mass eigenstates. In the usual 3 neutrino parameterization [?]

$$|U_{ei}|^2 = (c_{12}^2 c_{13}^2,\ s_{12}^2 c_{13}^2,\ s_{13}^2)\,, \tag{3.6}$$

where $c_{jk} = \cos\theta_{jk}$ and $s_{jk} = \sin\theta_{jk}$, being θ_{jk} the corresponding mixing angle. In our case, we use the best fit values $s_{12}^2 = 0.321$, $s_{13}^2 = 2.155\ (2.140) \times 10^{-2}$ for normal (inverted) ordering [?], see also [? ?] .

Finally, the factor $f_{c,i}\, n_0$ in equation (3.3) corresponds to the number density of the i-th mass eigenstate relic neutrino, where $f_{c,i}$ is the clustering factor, the local overdensity of these particles due to the gravitational attraction of our galaxy [? ? ?], and

$$n_\nu = \frac{3\zeta(3)}{4\pi^2} T_{\nu,0}^3 = 56\,\text{cm}^{-3} \tag{3.7}$$

is the number density without clustering, per neutrino and degree of freedom. It is obtained from a Fermi-Dirac distribution with a temperature $T_{\nu,0} \simeq 1.95\,\text{K}$.

Because of the experimental finite energy resolution, the main background to this process comes from the most energetic electrons of the β decay of tritium, since they can be measured

[1] The nuclear masses $m_{^3\rm He}$ and $m_{^3\rm H}$ are related to the atomic masses $M_{^3\rm He} \approx 2809.413\,\text{MeV}$ and $M_{^3\rm H} \approx 2809.432\,\text{MeV}$ [?] according to $m_{^3\rm He} = M_{^3\rm He} - 2m_e + 24.58678\,\text{eV}$ and $m_{^3\rm H} = M_{^3\rm H} - m_e + 13.59811\,\text{eV}$ (see the appendix of Ref. [?]).

with energies larger than the endpoint. To estimate the rate of such background, we need to account for the β decay spectrum [**?**]

$$\frac{d\Gamma_\beta}{dE_e} = \frac{\bar{\sigma}}{\pi^2} N_T \sum_{i=1}^{N_\nu} |U_{ei}|^2 H(E_e, m_i)\,, \tag{3.8}$$

where m_i is the mass of the i-th neutrino mass eigenstate. Defining $y = E_{\rm end,0} - E_e - m_i$, with $E_{\rm end,0}$ the energy at the β decay endpoint for massless neutrinos,

$$\begin{aligned} H(E_e, m_i) \;&= \frac{1 - m_e^2/(E_e m_{^3{\rm H}})}{(1 - 2E_e/m_{^3{\rm H}} + m_e^2/m_{^3{\rm H}}^2)^2} \sqrt{y\left(y + \frac{2m_i\, m_{^3{\rm He}}}{m_{^3{\rm H}}}\right)}\,\cdot \\ &\cdot \left[y + \frac{m_i}{m_{^3{\rm H}}}(m_{^3{\rm He}} + m_i)\right]\,. \end{aligned} \tag{3.9}$$

To account for the experimental energy resolution Δ, we introduce a smearing in the electron spectrum by convolving both, the CNB signal and the β decay spectrum with a Gaussian of full width at half maximum (FWHM) given by Δ. This relates with the standard deviation as

$$\sigma = \Delta/\sqrt{8\ln 2}. \tag{3.10}$$

The smeared neutrino capture event rate $\widetilde{\Gamma}_{\rm CNB}$ then reads

$$\frac{d\widetilde{\Gamma}_{\rm CNB}}{dE_e}(E_e) = \frac{1}{\sqrt{2\pi}\sigma} \sum_{i=1}^{N_\nu} \Gamma_i \times \exp\left\{-\frac{[E_e - (E_{\rm end} + m_i + m_{\rm lightest})]^2}{2\sigma^2}\right\}\,, \tag{3.11}$$

where $m_{\rm lightest}$ is the mass of the lightest neutrino and $E_{\rm end}$ is the energy at the β decay endpoint, $E_{\rm end} = E_{\rm end,0} - m_{\rm lightest}$. Similarly for the smeared β decays one finds

$$\frac{d\widetilde{\Gamma}_\beta}{dE_e}(E_e) = \frac{1}{\sqrt{2\pi}\sigma} \int_{-\infty}^{+\infty} dx\, \frac{d\Gamma_\beta}{dE_e}(x)\, \exp\left[-\frac{(E_e - x)^2}{2\sigma^2}\right]\,. \tag{3.12}$$

In Fig.s 1 and 2 we show the expected event rates at energies close to the β decay endpoint for different neutrino masses and energy resolutions. Of course, only the contributions of those neutrino masses larger than Δ can be resolved from the β decay background. Notice in the inverted ordering case (Fig. 2) a kink in the β decay spectra due to the larger overlap of ν_e with the heaviest mass eigenstates. In the normal ordering this feature can be hardly observed as ν_e has a much smaller mixing with ν_3. This is also the reason why the CNB capture peaks have different heights proportional to $|U_{ei}|^2$. For the smallest energy resolution we have considered, $\Delta = 0.01\,{\rm eV}$, one can also see the two contributions due to the sum of ν_1 and ν_2, and ν_3, respectively.

A good way to estimate the signal-to-noise ratio is to consider the events observed in an energy bin of width Δ and centered at the highest peak, that of ν_1, which has the maximal overlap with ν_e. The event rates in this bin for both signal and background are

$$\tilde{\Gamma}_{{\rm CNB},\nu_1}(\Delta) = \int_{E_{end,0}+m_1-\Delta/2}^{E_{end,0}+m_1+\Delta/2} \frac{d\tilde{\Gamma}_{\rm CNB}}{dE_e}\, dE_e, \tag{3.13}$$

$$\tilde{\Gamma}_\beta(\Delta) = \int_{E_{end,0}+m_1-\Delta/2}^{E_{end,0}+m_1+\Delta/2} \frac{d\tilde{\Gamma}_\beta}{dE_e}\, dE_e. \tag{3.14}$$

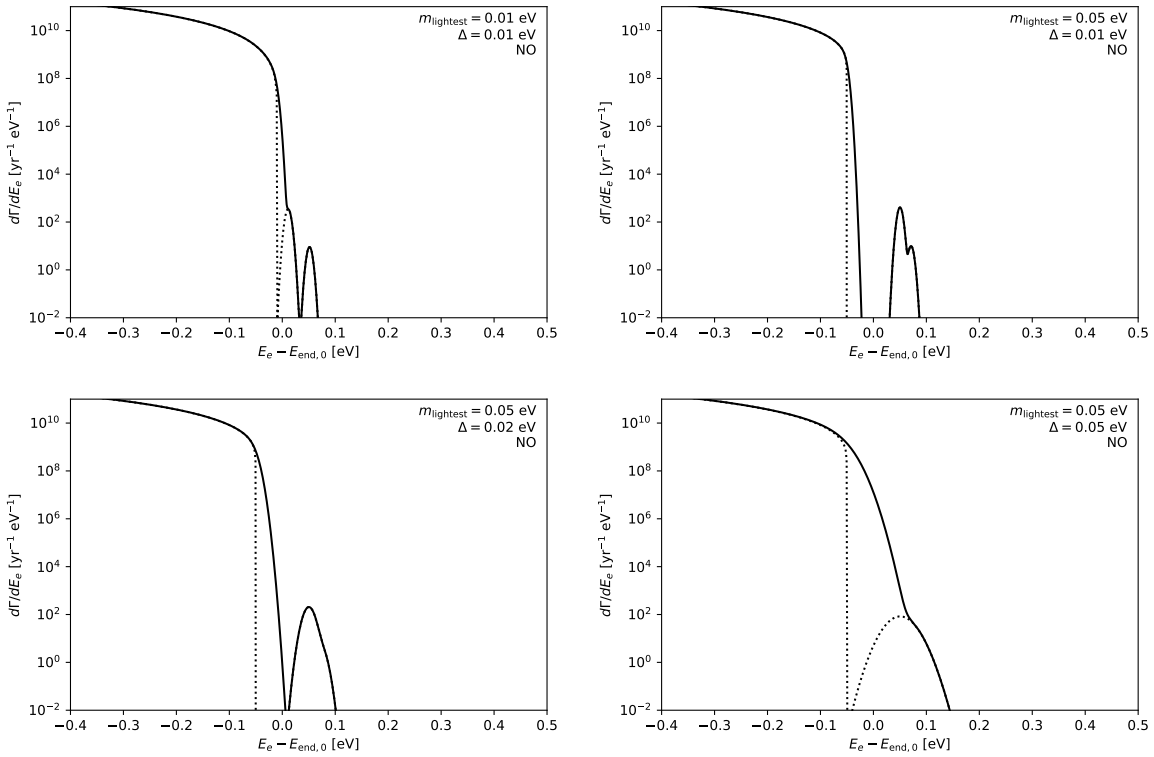

Figure 1. Expected event rates versus electron E_e in a direct-detection experiment near the β decay endpoint for different lightest neutrino masses and energy resolutions. Solid lines represent the event rates convolved with a Gaussian envelope of FWHM equal to the assumed energy resolution, as computed from Eqs. (3.11) and (3.12). Dotted lines show the same event rates without the convolution, i.e. $\Delta = 0$. Normal ordering of neutrino masses is assumed.

The signal-to-noise ratio is then

$$r_{\text{SN}} = \frac{\tilde{\Gamma}_{\text{CNB},\nu_1}(\Delta)}{\tilde{\Gamma}_{\beta}(\Delta)}. \tag{3.15}$$

Fig. 3 shows r_{SN} as a function of Δ and the lightest neutrino mass m_{lightest}. For large m_{lightest} the neutrino mass spectrum is in the degenerate region and both plots are the same. On the other hand, for lower m_{lightest} and a given Δ, the discovery potential is higher in the inverted mass ordering.

3.2 Neutrino mass sensitivity

To estimate the sensitivity of PTOLEMY to the neutrino mass scale we follow and adapt the procedure proposed in the KATRIN Design Report [**?**] and revisited from the Bayesian point of view in [**?**]. We consider here in details the standard active neutrino states and comment on how a similar analysis might also be applied to extra sterile states with mass in the eV and keV ranges, suggested by neutrino oscillation anomalies or proposed as warm DM candidates, respectively.

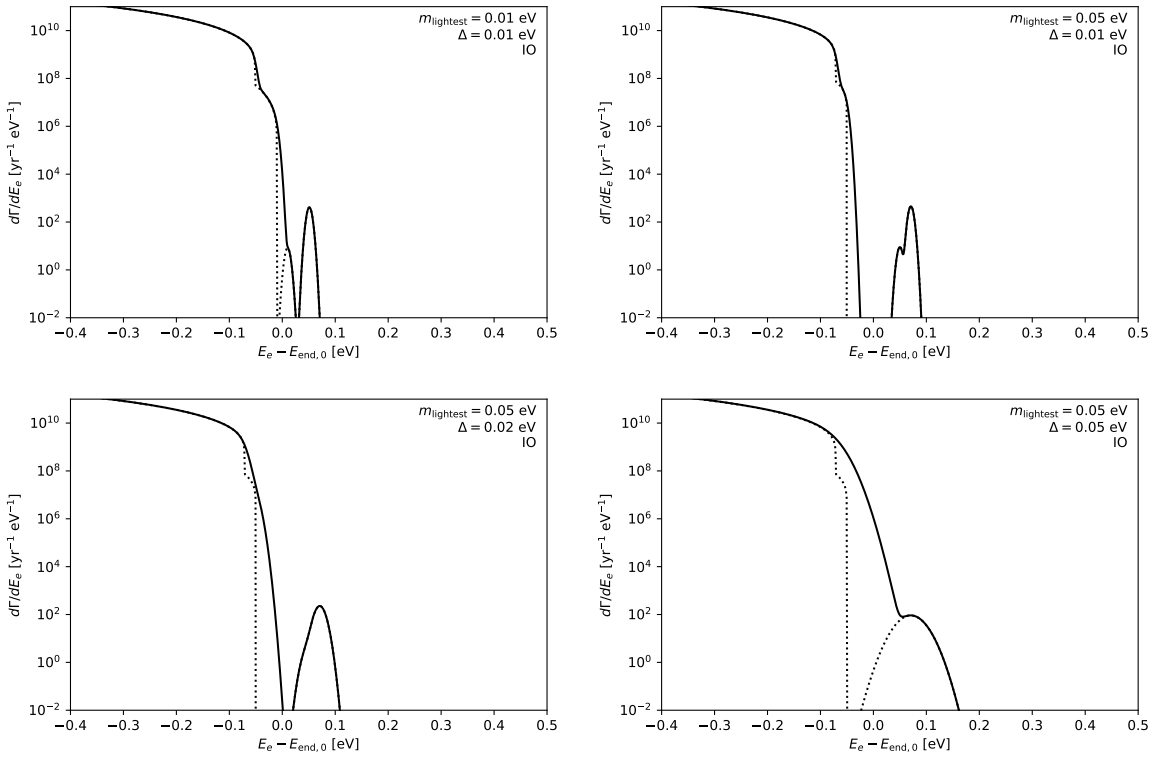

Figure 2. Same as Fig. 1 but for inverted ordering of neutrino masses.

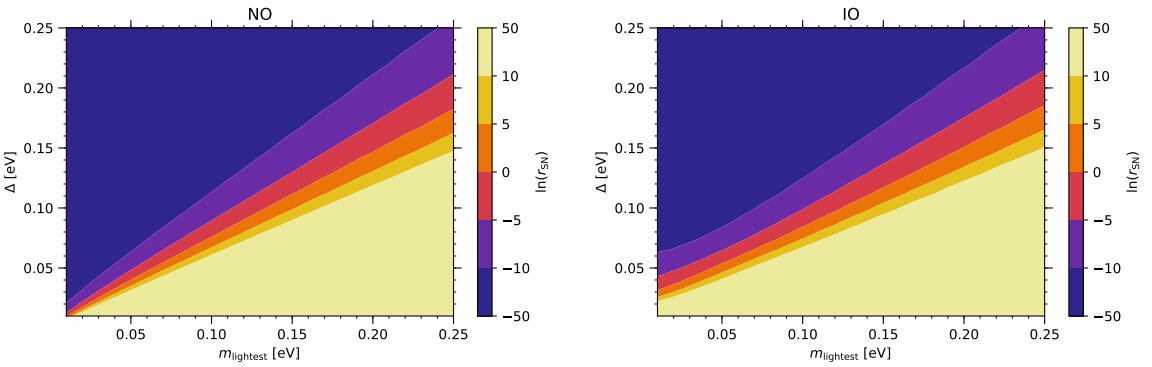

Figure 3. Signal-to-noise ratio for relic neutrino capture as defined in Eq. (3.15) for different values of the energy resolution and the mass of the lightest neutrino. Left (right) panel shows the result for normal (inverted) ordering.

Following the notation adopted in the previous section, we define the number of β decay and neutrino capture events within an energy bin centered at E_i as

$$N_\beta^i = T \int_{E_i-\Delta/2}^{E_i+\Delta/2} \frac{d\widetilde{\Gamma}_\beta}{dE_e} dE_e \,, \tag{3.16}$$

$$N_{\rm CNB}^i = T \int_{E_i-\Delta/2}^{E_i+\Delta/2} \frac{d\widetilde{\Gamma}_{\rm CNB}}{dE_e} dE_e \,, \tag{3.17}$$

with T the exposure time. In our Bayesian simulation we reconstruct the physical parameters given an initial fiducial model. For the fiducial models we will vary the masses ($\hat{m}_i$) and mixing matrix ($\hat{U}$) parameters, as well as the true endpoint of the β spectrum ($\hat{E}_{\rm end}$) according to the currently known best fit values [2].

For the fiducial model, the number of expected events per energy bin is given by:

$$\hat{N}^i = N^i_\beta(\hat{E}_{\rm end}, \hat{m}_i, \hat{U}) + N^i_{\rm CNB}(\hat{E}_{\rm end}, \hat{m}_i, \hat{U})\,. \tag{3.18}$$

The total number of events that will be measured in a bin is the sum of $\hat{N}^i$ and of a constant background:

$$N^i_t = \hat{N}^i + \hat{N}_b\,, \tag{3.19}$$

where $\hat{N}_b = \hat{\Gamma}_b T$ with $\hat{\Gamma}_b$ the fiducial PTOLEMY background rate, adopted to be 10^{-5} Hz over the entire energy range under consideration. In this first phase we estimate the experimental measurement in each energy bin as:

$$N^i_{\rm exp}(\hat{E}_{\rm end}, \hat{m}_i, \hat{U}) = N^i_t \pm \sqrt{N^i_t}\,, \tag{3.20}$$

assuming a statistical error of $\sqrt{N^i_t}$ in each bin. Systematic errors will be studied using dedicated Montecarlo simulations once the detector design will be more defined. In a second phase we also plan to implement more sophisticated statistical simulations using the following expression to estimate the experimental measurements

$$N^i_{\rm exp}(\hat{E}_{\rm end}, \hat{m}_i, \hat{U}) = \begin{cases} Rnd[\text{Poisson}(N^i_t)] & \text{if } N^i_t < 1000 \\ Rnd\left[\text{Gauss}\left(\mu = N^i_t, \sigma = \sqrt{N^i_t}\right)\right] & \text{if } N^i_t \geq 1000 \end{cases}\,. \tag{3.21}$$

The simulated measurement is fitted in order to reconstruct the values of the theoretical parameters that describe the physical model. We introduce a normalization uncertainty on the number of β events (A_β), on the endpoint energy (ΔE_{end}) and an unknown constant background (N_b). These parameters will be determined by the fit. In order to test the perspectives for CNB detection, we multiply the capture event number by an unknown normalization $A_{\rm CNB}$, whose baseline value is one. A direct detection of the CNB at a given C.L. can then be claimed if $A_{\rm CNB}$ is found to be incompatible with zero at that C.L..

For sake of brevity, in the following we will indicate the list of theoretical parameters with $\boldsymbol{\theta} = (A_\beta, N_b, \Delta E_{end}, A_{\rm CNB}, m_i, U)$.

The theoretical number of events in the bin i therefore reads

$$\begin{aligned} N^i_{\rm th}(\boldsymbol{\theta}) \;=\; & A_\beta N^i_\beta(\hat{E}_{end} + \Delta E_{end}, m_i, U) \\ & + A_{\rm CNB} N^i_{\rm CNB}(\hat{E}_{end} + \Delta E_{end}, m_i, U) + N_b\,. \end{aligned} \tag{3.22}$$

In order to perform the analysis and fit the desired parameters $\boldsymbol{\theta}$, we use the following χ^2 function:

$$\chi^2(\boldsymbol{\theta}) = \sum_i \left(\frac{N^i_{\rm exp}(\hat{E}_{\rm end}, \hat{m}_i, \hat{U}) - N^i_{\rm th}(\boldsymbol{\theta})}{\sqrt{N^i_t}} \right)^2\,, \tag{3.23}$$

which will be converted into a likelihood function $\mathcal{L}$ for the Bayesian analysis according to $\chi^2 = -2\log\mathcal{L}$.

[2] When considering the case of sterile states, one should also add a fiducial mass m_4, mixing angle and cosmological number density as suggested by oscillation anomalies and allowed by cosmological data.

In the following series of simulations, we always consider 100 g mass for the tritium source, one year of data taking, an observed energy range between $\hat{E}_{\rm min} = E_0 - 5$ eV and $\hat{E}_{\rm max} = E_0 + 10$ eV and a constant background rate $\Gamma_b = 10^{-5}$ Hz over the whole energy range. We have verified that increasing $\hat{E}_{\rm max}$ has no impact on the results, while some effect may come from a different $\hat{E}_{\rm min}$. If $\hat{E}_{\rm min}$ is decreased, the precision in measuring the β spectrum (its normalization and the endpoint) allows to slightly improve the sensitivity on the neutrino parameters, but this comes at the price of a larger number of events, which might be difficult to handle. On the other hand, a $\hat{E}_{\rm min}$ closer to the endpoint allows to reduce the β decay event rate at the expense of slightly worsening the precision on the neutrino mass. The best value for $\hat{E}_{\rm min}$ will be determined once the technical properties of the apparatus is defined more precisely.

A further comment regards the constant background rate $\hat{\Gamma}_b$. For an amount of tritium of 100 g, the number of events expected from the β decay is much larger than the background rate and the determination of the neutrino masses or the detection of a putative sterile neutrino will be possible even with a much larger $\hat{\Gamma}_b$. In other words, a much smaller tritium mass might be sufficient to get a sensitivity on neutrino mass scale of the order of 0.1 eV or less. Yet, a 100 g mass and $\hat{\Gamma}_b \lesssim 10^{-5}$ Hz, are crucial to allow a detection of the relic neutrinos, which remains the primary purpose of PTOLEMY.

To perform the analysis, we have adapted the generic Markov Chain Monte Carlo (MCMC) sampler used in `CosmoMC` [**?**]. The theoretical parameters that we will try to reconstruct are: the lightest neutrino mass $m_{\rm lightest}$, and, for scenarios with an extra sterile neutrino state, the squared mass difference Δm^2_{41} and the mixing angle s^2_{14}.

PTOLEMY is expected to have impressive performances in reconstructing the fiducial value for the lightest neutrino mass. The 1σ statistical error obtained from the simulations is of the order of 10^{-3} eV or below, with minimal dependences on the detector configurations studied here, energy range and background rate. Reasonably, the error slightly depends on the energy resolution of the experiment and on the value of the fiducial lightest neutrino mass, with smaller relative errors for larger masses. This can be seen in Fig. 4, where we show relative statistical errors obtained when reconstructing a given fiducial lightest neutrino mass $\hat{m}_{\rm lightest}$, adopting different energy resolutions Δ and 100 g yr of PTOLEMY data. As we can see, PTOLEMY will distinguish the neutrino mass almost independently of the experimental energy resolution, which only influences slightly the magnitude of the statistical error. The reason is that a larger lightest neutrino mass does not only induce a shift in the endpoint of the β decay spectrum, but also a change in the normalization of the spectrum at all energies, which can be measured very well thanks to the very large event rate.

Along with mass reconstruction, we can also study the possibility to detect the CNB capture events. As already mentioned, we fit the signal from CNB capture using a free normalization $A_{\rm CNB}$ and we can claim a detection if $A_{\rm CNB}$ can be distinguished from zero. Figure 5 shows the C.L. which can be achieved as a function of the different fiducial lightest neutrino masses and energy resolutions. As we can see, it is crucial to achieve a very good energy resolution, but this may be not enough if the neutrino masses are very small and the ordering of the mass eigenstates is normal.

Another interesting result that PTOLEMY can obtain is the determination of the neutrino mass ordering. This is due to the fact that the shape of the β spectrum near the endpoint depends on the single mass eigenstates and on the mixing matrix elements as described in eq. (3.8) and already shown in Fig.s 1 and 2. Currently, neutrino oscillations data prefer normal ordering (NO, $\Delta m^2_{31} > 0$) over the inverted one (IO, $\Delta m^2_{31} < 0$) [**?**].

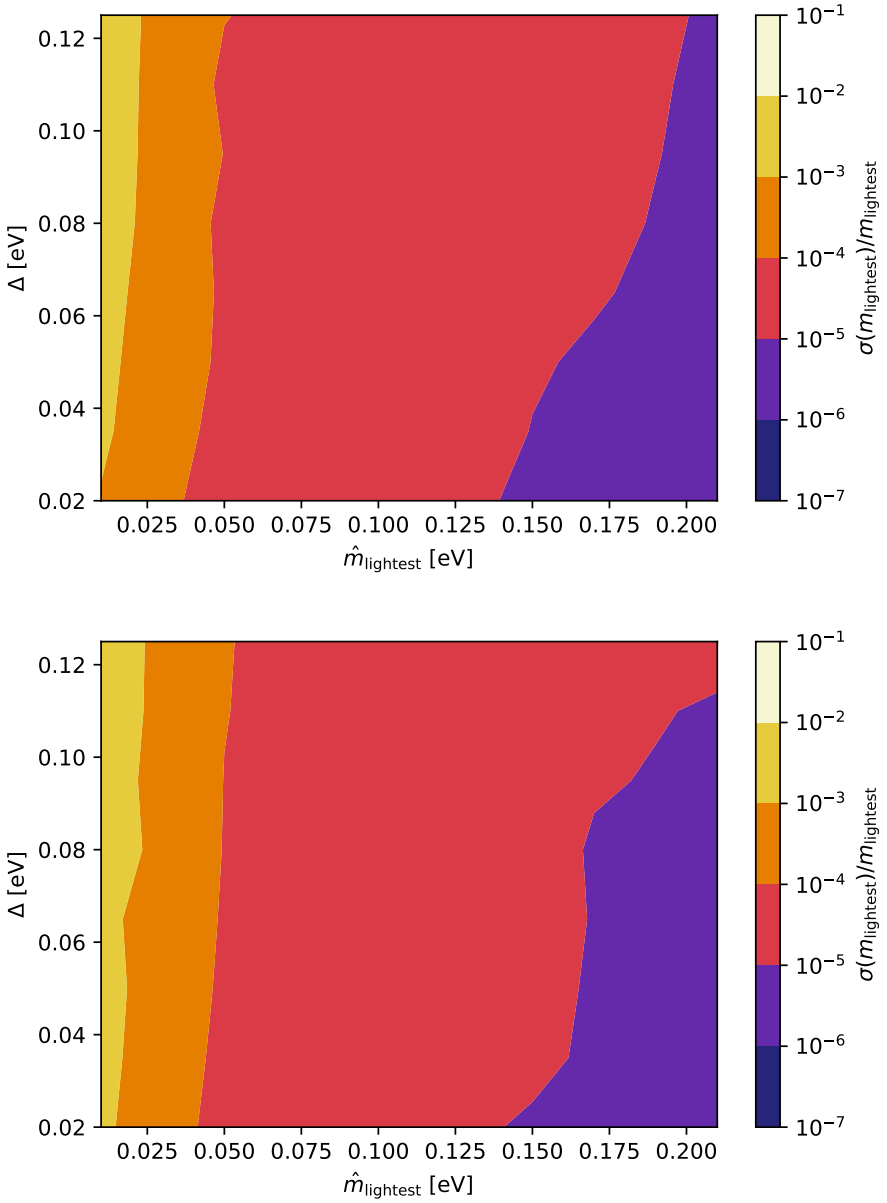

Figure 4. Relative error on the reconstructed lightest neutrino mass $m_{\rm lightest}$ as a function of the fiducial lightest neutrino mass $\hat{m}_{\rm lightest}$ and the energy resolution Δ, considering 100 g yr of PTOLEMY data. The top (bottom) panel represents normal (inverted) ordering of the neutrino mass eigenstates.

To estimate the capabilities of PTOLEMY in determining the mass ordering, we perform two sets of simulations, assuming as fiducial values the best-fit mixing parameters obtained within NO or IO [**?**] respectively. For each of the two cases, we fit the simulated experimental data using both the NO and IO best-fit mixing parameters and we compute the Bayesian evidence $\mathcal{Z}$ [3]. We will then have four cases: fiducial NO fitted using NO ($\widehat{\rm NO}$/NO for sake

[3]For a review on Bayesian model comparison see e.g. [**?**], for its application in determining the neutrino mass ordering see [**?**].

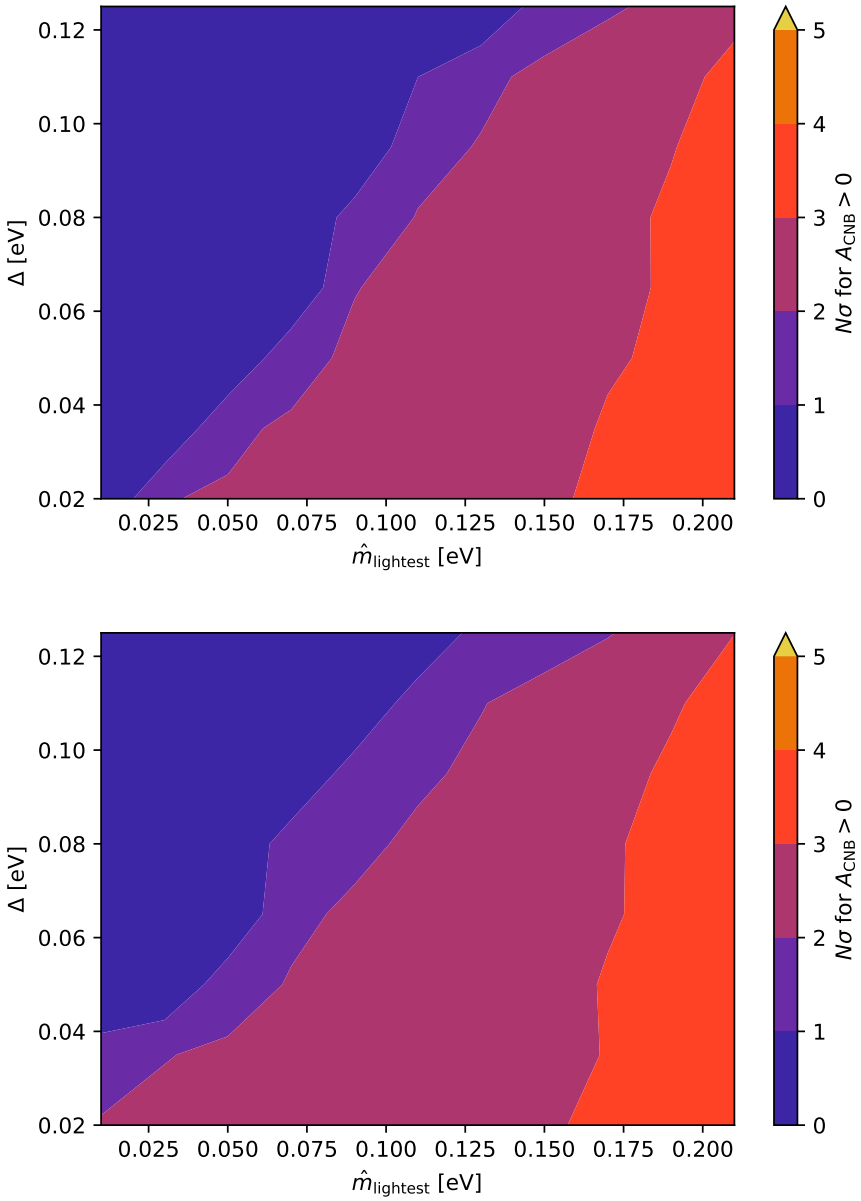

Figure 5. Statistical significance for the detection of the CNB as a function of the fiducial lightest neutrino mass $\hat{m}_{\text{lightest}}$ and the energy resolution Δ, considering 100 g yr of PTOLEMY data. The top (bottom) panel represents normal (inverted) ordering of the neutrino mass eigenstates.

of brevity), fiducial NO fitted using IO ($\widehat{\text{NO}}$/IO), fiducial IO fitted using NO ($\widehat{\text{IO}}$/NO) and fiducial IO fitted using IO ($\widehat{\text{IO}}$/IO). The PTOLEMY sensitivity on the mass ordering is then determined using the Bayes factor:

$$\ln \mathcal{B}_{ij} = \ln \mathcal{Z}_i - \ln \mathcal{Z}_j \,. \tag{3.24}$$

The magnitude of the Bayes factor indicates the strength of the preference for one of the two competing cases, while the sign of $\ln \mathcal{B}_{ij}$ indicates which of the two cases is preferred (case i

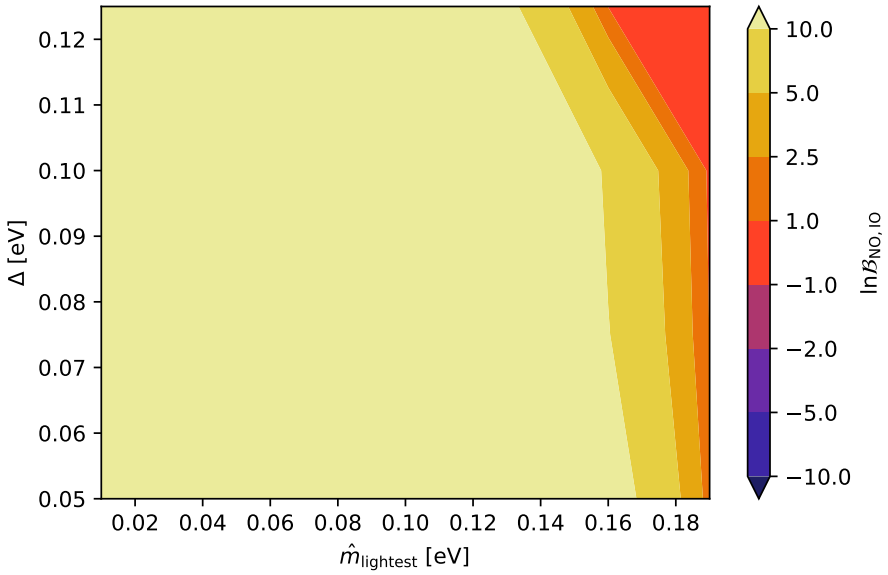

Figure 6. Statistical significance for the determination of the neutrino mass ordering, if the NO is assumed as true, as a function of the fiducial lightest neutrino mass $\hat{m}_{\rm lightest}$ and the energy resolution Δ, considering 100 g yr of PTOLEMY data. Positive values of $\ln \mathcal{B}_{NO,IO}$ correspond to a preference for NO, which is statistically decisive if $\ln \mathcal{B}_{NO,IO} > 10$.

if $\ln \mathcal{B}_{ij} > 0$, case j if $\ln \mathcal{B}_{ij} < 0$). If PTOLEMY is able to distinguish the two orderings, we expect the fits performed using the same case as the fiducial ($\widehat{\rm NO}$/NO, $\widehat{\rm IO}$/IO) to be better than the ones that assume an opposite ordering with respect to the fiducial one ($\widehat{\rm NO}$/IO, $\widehat{\rm IO}$/NO). As a consequence, we expect

$$\ln \mathcal{B}^{\widehat{NO}}_{NO,IO} \equiv \ln \mathcal{Z}_{\widehat{\rm NO}/{\rm NO}} - \ln \mathcal{Z}_{\widehat{\rm NO}/{\rm IO}} > 0\,, \tag{3.25}$$

$$\ln \mathcal{B}^{\widehat{IO}}_{NO,IO} \equiv \ln \mathcal{Z}_{\widehat{\rm IO}/{\rm NO}} - \ln \mathcal{Z}_{\widehat{\rm IO}/{\rm IO}} < 0\,. \tag{3.26}$$

In Fig. 6 we show $\ln \mathcal{B}^{\widehat{NO}}_{NO,IO}$ as a function of the fiducial lightest neutrino mass $\hat{m}_{\rm lightest}$ and the energy resolution Δ. As we can see, PTOLEMY will be capable of determining the mass ordering (if it is normal) in the non-degenerate region, while the distinction will not be feasible ($\ln \mathcal{B}_{NO,IO}$ is inconclusive) for neutrino masses above ~ 0.18 eV.

Another aspect related to mass ordering is that the direct detection of relic neutrinos is generally easier for IO than for NO. As we already mentioned, this is due to the fact that the primary CNB peaks are shifted at higher electron energies, because m_1 and m_2 are larger (see figs. 1 and 2). As a result, the perspectives of CNB detection at small neutrino masses are improved in IO with respect to NO, see the bottom panel of Fig. 5.

3.3 Sterile neutrinos

We have also considered a more exotic scenario with an extra sterile neutrino specie ν_4 with mass around the eV.

Data from both BBN and CMB are incompatible with a fully thermalized sterile neutrino with an eV mass and mixing angle required to solve the three oscillation neutrino anomalies. In fact, this would turn into a larger radiation content in the early universe, a faster expansion rate given by the Hubble factor, which would change both primordial deuterium (and to a less extent ^{4}He) produced during BBN [**?**] and the relative distance of the first acoustic peak and the damping tail in the CMB power spectrum [**? ?**]. These observations constrain the sterile state number density to a factor 0.5-0.6 with respect to the active neutrino one $n_\nu = 56$ cm^{-3}. The feasibility of the measurement is strictly related to the theoretical model under consideration, accounting for sterile neutrino clustering effects, which might be quite relevant [**?**].

On the other hand, the measurements of the β spectrum will be extremely useful to put bounds on the new squared mass difference Δm^2_{14} and mixing angle s^2_{14} through the suppression of the spectrum at energies above $\sim \sqrt{\Delta m^2_{14}}$ emerging from eq. (3.8). Given the current indication coming from model-independent short baseline neutrino oscillations at the DANSS and NEOS reactor experiments, the forth neutrino mass eigenstate may have a mass defined by $\Delta m^2_{14} \simeq 1.29$ eV^2 and a mixing angle $s^2_{14} \simeq 0.012$ [**?**], PTOLEMY will be able to reconstruct the fiducial values with uncertainties at the level of 10^{-4} for both $\log_{10}(\Delta m^2_{14}/\text{eV}^2)$ and $\log_{10}(s^2_{14})$. When fitting a fiducial model with $\Delta m^2_{14} = 0$ and $s^2_{14} = 0$, we can obtain a marginalized 3σ limit $s^2_{14} \lesssim 10^{-4}$. In this case it is very useful to be able to measure a larger fraction of the β-decay energy spectrum, since the suppression corresponding to the forth neutrino starts to be relevant at energies $\sim E_0 - \sqrt{\Delta m^2_{14}}$. Being able to determine the normalization below and above this point would help to discriminate the effect of the sterile neutrino from other effects.

In Fig. 7 we show the perspectives for detecting a light fourth neutrino mass eigenstate with a small mixing with the electron neutrino, considering a wide range of fiducial new squared mass differences and mixing angles. While for very small mixing angles PTOLEMY will not be able to distinguish the effect of a new kink in the β spectrum, a detection will be clearly possible given the current preferred values of the best-fit mixing parameters (see e.g. [**? ? ?**]).

In the future we plan to address a similar analysis for the case of a sterile neutrino with mass in the keV range, which has been considered as a warm DM candidate. If we assume that the whole DM is made by such particles, their local energy density would be of order GeV cm^{-3}, i.e. a pretty large local number density of 10^5 cm^{-3}, while their average density on cosmological scales is five order of magnitude smaller. This means that the sterile states cannot have been produced in equilibrium in the early universe. This, together with astrophysical constraints, bounds the sterile-active mixing angle to be very small, $\sin^2\theta_{i4} \leq 10^{-8}$ [**?**]. We thus, expect the sterile neutrino capture signal to be too small to be detected by PTOLEMY, while the analysis of the much larger event number expected in the β decay spectrum might provide bounds on both m_4 and mixing angles.

4 Directional Detection of MeV Dark Matter

The development goals of high radio-purity graphene targets are two-fold. The first is to yield a low background target for the CNB measurement, and the second is for the deployment of high sensitivity detectors using the unique properties of graphene. The proposal is to focus initially on the latter goal and to conduct a significant MeV dark matter search with novel graphene-based detectors [**? ?**]. The count rate requirements are more stringent for MeV

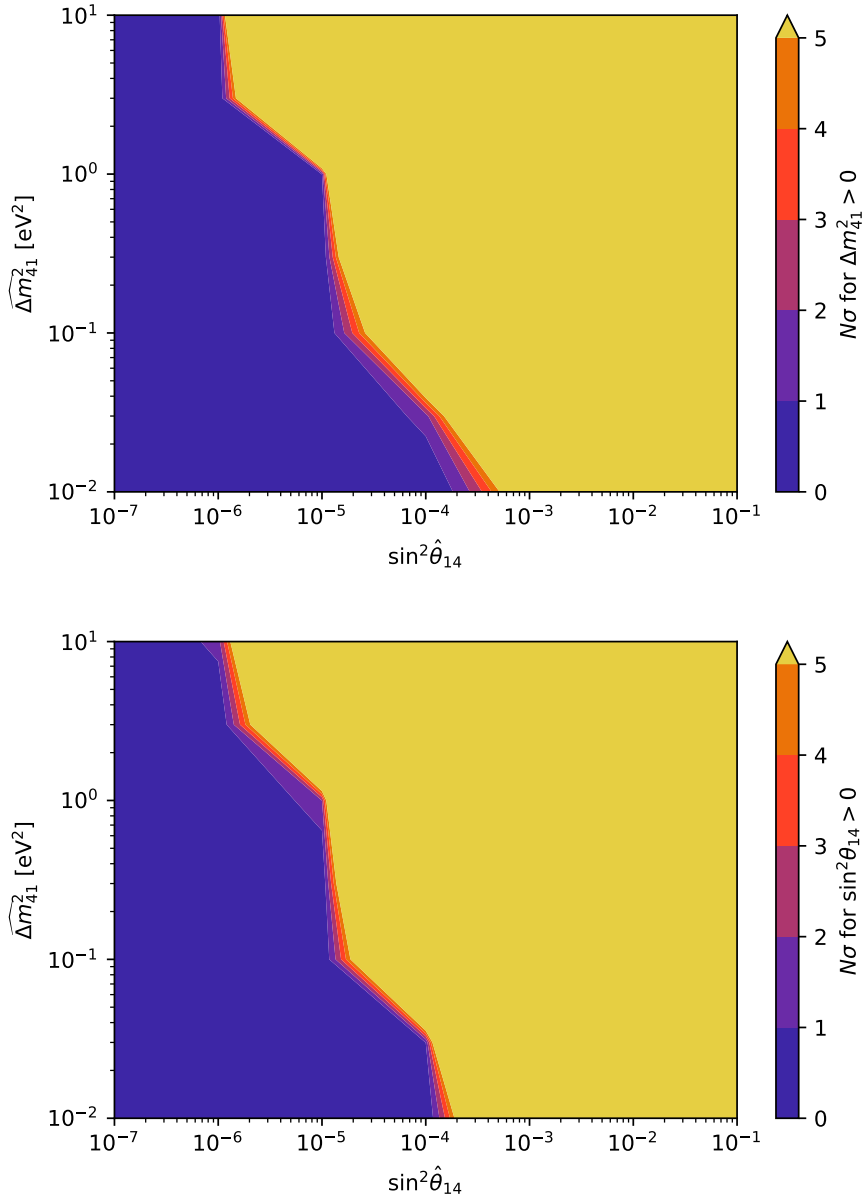

Figure 7. Statistical significance for a detection of a fourth neutrino mass eigenstate from measurements of the β spectrum, assuming various fiducial values for the new squared mass difference and mixing angle, considering 100 g yr of PTOLEMY data. The top (bottom) panel depicts the perspectives for Δm^2_{41} ($\sin^2\theta_{14}$).

dark matter searches due to the broad energy spectrum of low energy recoil electrons, as described below.

There are two approaches to directional detection MeV dark matter(DM) searches that will be investigated with the PTOLEMY prototypes. One of them, called PTOLEMY-G^3, self-instruments the graphene target at the level of single electron sensitivity. This extraordinary level of sensitivity enables the detector to sense low levels of radio-impurities through-

out the target volume without the need of a magnetic spectrometer. The second is a carbon nanotube(CNT) detector, called PTOLEMY-CNT herein, that leverages the anisotropic scattering and absorption properties of tightly packed, aligned CNTs to determine the scattering direction of MeV dark matter. The advantage of this approach is in the large scale increase in graphene mass that is achieved with this approach, while still maintaining sensitivity to the forward-backward scattering cross section asymmetry imposed by the direction of the dark matter wind.

5 PTOLEMY-G^3

With a small-scale deployment of PTOLEMY-G^3 [**?**], based on G-FET sensors, a fiducialized volume of 10^3 cm^3 consisting of 100 stacked 4-inch wafers will search down to approximately $\bar{\sigma}_e = 10^{-33}$ cm^2 for dark matter masses of 4 MeV in one year, uncovering a difficult blind spot inaccessible to current nuclear recoil experiments (see Fig. 8). This new approach will open up for the first time direct directional detection of MeV dark matter (see Fig. 9), a capability that no other light dark matter proposal has and which would be highly complementary to a detection, for example, in DAMIC or SENSEI. The graphene target will follow high radio-purity wafer-level fabrication procedures [**?**]. The support structures will use materials that have achieved high radio-purity [**?**].

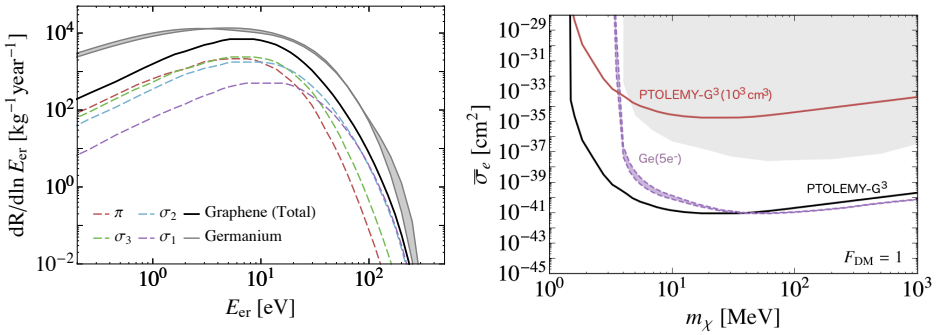

Figure 8. (*left*) Differential rate for a 100 MeV DM particle scattering off an electron in graphene is shown with the solid black line with $\bar{\sigma}_e = 10^{-37}$ cm^2 and $F_{\rm DM}(q) = 1$. (*right*) Expected background-free 95% C.L. sensitivity for a graphene target with a 1-kg-year exposure (black). A first experiment with a G^3 volume of 10^3 cm^3 (target surface of 10^4 cm^2) will search down to approximately $\bar{\sigma}_e = 10^{-33}$ cm^2 at 4 MeV.

The G-FET sensor has a tunable meV band gap (see Fig. 10), a full three orders of magnitude smaller than cryogenic germanium detectors. This sensitivity is used to switch on and off the conductivity of the G-FET channel by 10 orders of magnitude in charge carriers in response to the gate voltage shift from a single scattered electron. A narrow, vacuum-separated front-gate imposes kinematic discrimination on the maximum electron recoil energy, where low energy recoil electrons above the graphene work function follow FET-to-FET directional trajectories within layers of the fiducialized G^3 volume. Each FET plane will be vacuum sealed on top and bottom during assembly. The target will be kept at cryogenic temperatures and have no line-of-sight vacuum trajectories from the outer vacuum region to the sealed FET planes. Residual gas backgrounds will be cryopumped to the outer boundaries of the fiducialized volume.

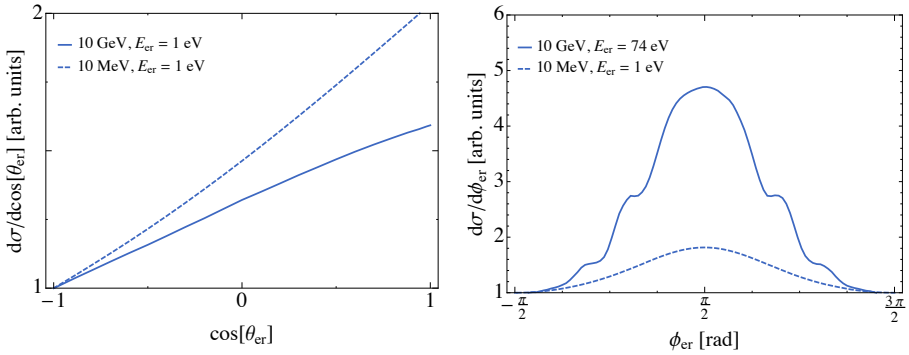

Figure 9. Predicted angular distributions for DM masses 10 MeV (dashed) and 10 GeV (solid) in a DM stream with $v_{\rm stream} = 550$ km/s in the lab frame. (*left*) Polar distribution of the final-state electron when the stream is oriented perpendicular to the graphene plane and points along $\cos\theta = 1$. (*right*) Azimuthal distribution of the final-state electron when the stream is oriented parallel to the graphene plane and points along $\phi = \pi/2$. The outgoing electron direction is highly correlated with the initial DM direction.

The fine segmentation of the G-FETs provide localization of backgrounds and the FET-to-FET coincidence further suppresses the background count rate. The intrinsic ^{14}C background from the graphene target will profit from a newly identified source of CO_2 that is estimated to be three orders of magnitude lower in $^{14}C/^{12}C$ than achieved in Borexino. This source was recently identified in the collection of low background underground Argon. The AMS methods for verifying low-level $^{14}C/^{12}C$ are described in [**?**], and the AMS facilities described in this paper are now located at the Lalonde AMS Lab at the University of Ottawa. The fabrication process to implement high radio-pure CO_2 to grow the graphene target is described in the high radio-pure ^{12}C WP.

6 PTOLEMY-CNT

The physics reach for MeV dark matter and the principles of operation of the carbon nanotube(CNT) target are described in [**?**]. The path of propagation of scattered low energy electrons through the CNT target is depicted schematically in Fig. 11. The directionality derives from the forward-backward anisotropy of the dark matter cross section stemming from the dark matter wind direction relative to the open-end of the CNT target orientation. A low energy electron exiting the CNT target through the open-end will be accelerated into a single electron detector through an applied voltage potential. Measurements of the graphene-electron interactions, including transmission, absorption and scattering, indicate that the electrons produce in the CNT target will have a high transparency to reach the end of the CNT target for direct detection of the electrons. The characterization of these properties is the focus of the graphene work package.

Fig. 12 shows the recoil energy spectrum of electrons from 5 MeV dark matter scattering in the CNT. The cross section sensitivity to MeV dark matter for a CNT mass exposure of $M \cdot t$(kg·day)$\simeq$ 16 reaches a sensitivity of $\bar{\sigma}_e = 10^{-37}$ cm^2 for dark matter masses of 5 MeV owing the relatively large target mass that can be achieved in the CNT configuration. The physics reach for a 1-kg-year exposure is shown in Fig. 12.

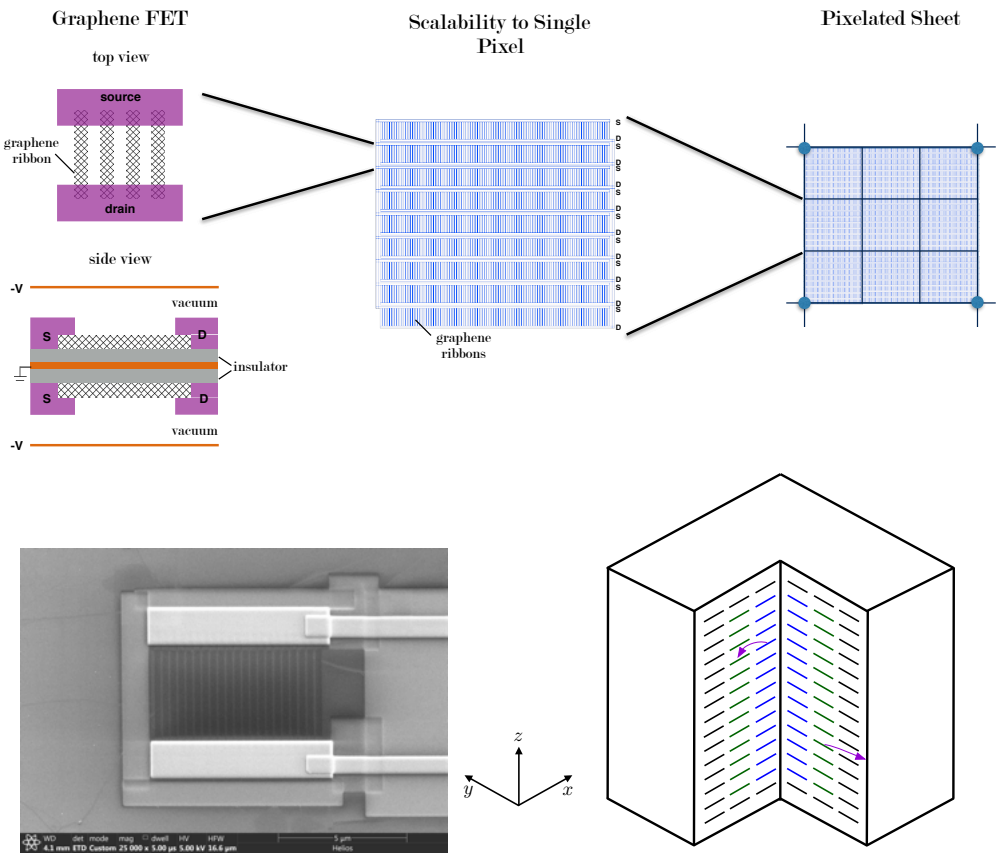

Figure 10. (*top*) The FET plane will be double-sided, separated by two insulating layers and a bottom gate electrode. Top gate electrodes will provide the ~ -100 V needed to accelerate ejected electrons away from the electrodes and back towards the graphene planes. Multiple graphene FETs can be arranged into a single pixel (center) with interdigitated source and drain and multiple pixels are arranged into sheets that are stacked together to form a cube structure and multiple cubes are assembled to form a fiducialized volume. (*left bottom*) Prototype graphene FET sensor made at Princeton University consists of a source and drain separated by a planar graphene layer segmented finely into ribbons. (*right bottom*) Cutaway view of a conceptual design for graphene directional detection. When an electron is ejected from a graphene sheet, it is deflected by an electric field, where electrons follow a "FET-to-FET" trajectory.

Acknowledgments

This is the most common positions for acknowledgments. A macro is available to maintain the same layout and spelling of the heading.

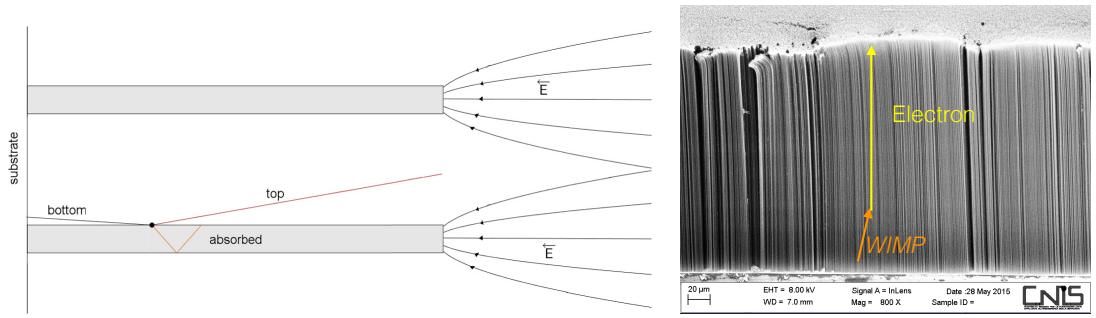

Figure 11. (*left*) Angular directionality from the CNT target depends on the orientation of the CNTs (shown here horizontally) relative to the dark matter wind. A voltage potential at the open-end of the CNTs accelerate the low energy recoil electrons into a single electron sensor. (*right*) SEM image of densely packed CNTs (oriented vertically).

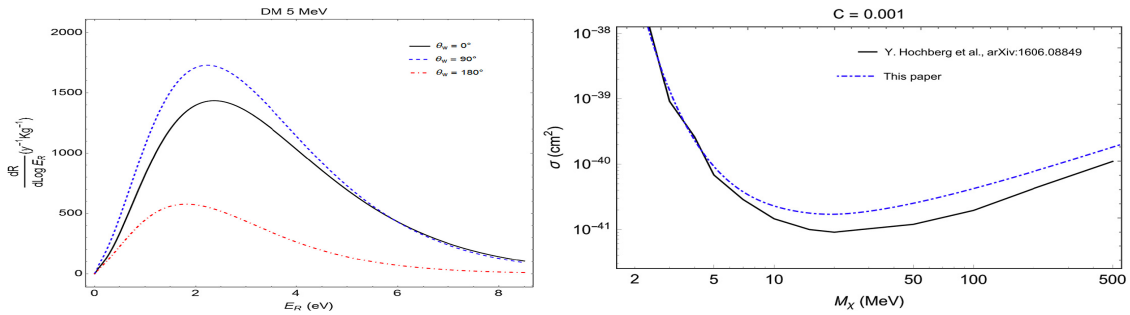

Figure 12. (*left*) Differential rate for a 5 MeV DM particle scattering off an electron in the CNT target is shown. (*right*) Expected background-free 95% C.L. sensitivity for the CNT target with a 1-kg-year exposure.